Initial Conditions for Surface Hopping Trajectories from the VSCF-Wigner distribution

R. Cvjetinović,[1,2] J. Odavić,[3,4] R. Ćosić,[5] M. Sapunar,[1,a)] and N. Došlić[1,b)]

[1)] *Division of Physical Chemistry, Ruđer Bošković Institute, Bijenička cesta 54, 10000 Zagreb, Croatia*

[2)] *Faculty of Science, Department of Chemistry, University of Zagreb, Horvatovac 102a, Zagreb 10000, Croatia*

[3)] *Dipartimento di Fisica "Ettore Pancini", Università degli Studi di Napoli "Federico II", Complesso Universitario di Monte Sant'Angelo, Via Cinthia, 21, Napoli, 80126, Italy*

[4)] *Istituto Nazionale di Fisica Nucleare (INFN), Sezione di Napoli, Complesso Universitario di Monte Sant'Angelo, Via Cinthia, 21, Napoli, 80126, Italy*

[5)] *IT4Innovations, VSB – Technical University of Ostrava, 17. listopadu 2172/15, 708 00 Ostrava-Poruba, Czech Republic*

(Dated: 27 February 2026)

In trajectory surface hopping (TSH) simulations, initial conditions are typically generated using harmonic Wigner distributions, which assume independent harmonic normal modes. While this assumption fails for anharmonic systems, it remains unclear under which conditions harmonic Wigner sampling becomes unreliable in photochemical simulations and whether anharmonicity alone is a sufficient criterion for reconsidering the use of harmonic Wigner sampling. In the present study, we introduce a sampling strategy based on vibrational self-consistent field (VSCF) theory to construct a VSCF Wigner quasiprobability distribution that incorporates anharmonic effects while retaining mode separability. Analytical expressions are derived in both harmonic and distributed Gaussian bases enabling the implementation in TSH simulations. The method is applied to malonaldehyde and methylhydroperoxide, which exhibit moderate and strong anharmonicity, respectively. For malonaldehyde, VSCF-based and harmonic Wigner sampling yield similar results, indicating that harmonic Wigner sampling remains reliable despite the anharmonicity. In methylhydroperoxide (MHP), where torsional motion strongly influences the excited-state character, VSCF Wigner sampling gives results comparable to the quantum thermostat approach while offering a computationally efficient and systematically improvable route to initial-condition sampling.

[a)]Electronic mail: msapunar@irb.hr
[b)]Electronic mail: nadja.doslic@irb.hr

I. INTRODUCTION

In photoinduced processes, a sudden change of the electronic state of a system often leads to the breakdown of the Born-Oppenheimer approximation. For this reason, the treatment of nonadiabatic effects is critical for successful simulations in photochemistry. For this task, trajectory surface hopping (TSH) methods are often the method of choice since they retain the efficiency of classical trajectories while successfully describing the population dynamics in excited state processes. The driving idea behind TSH simulations is to partially include quantum effects on top of classical trajectories.[1,2] While the primary purpose of TSH is to account for nonadiabatic effects that arise when potential energy surfaces (PESs) become degenerate near conical intersections, a natural question that arises is whether other nuclear quantum effects, specifically zero point energy, can also be incorporated.

Methods based on trajectories (or trajectory basis functions) require well-defined positions and momenta of the nuclei. The closest quantum mechanical equivalent to the phase space distribution is the Wigner quasiprobability distribution which fully describes the state of a quantum system in the phase space representation.[3] Sampling initial conditions from this distribution is not straightforward because 1) it is difficult to numerically evaluate the true Wigner distribution and 2) it is not a true probability distribution and has negative regions causing problems for methods based on classical trajectories.[4–9] The method introduced in this work addresses these issues. However, even in the ideal case where the initial conditions perfectly reflect the quantum distribution, classical trajectories will not preserve the correct zero point energy distribution over time.[10] This issue is beyond the scope of this work, but is usually not considered a major problem over the very short time scales typically encountered when studying the first phase of photochemical reactions.

The most common method for selecting initial conditions for TSH simulations of small to medium sized molecules is sampling from the harmonic Wigner quasiprobability distribution. This method is usually referred to simply as Wigner sampling, but going forward we will use the term "harmonic Wigner sampling" to differentiate from the "VSCF Wigner sampling" introduced here. Harmonic Wigner sampling involves two assumptions which greatly simplify the problem: that the normal modes are independent and that the potential along them is truly harmonic. The former approximation allows the full Wigner distribution to be expressed as a product of independent single mode distributions, which can then be sam-

pled independently, avoiding the curse of dimensionality. The latter approximation allows the Wigner distribution to be written in a simple analytical form that depends only on the frequency of the normal mode and remains strictly positive for both the vibrational ground state and a system in thermal equilibrium. Taken together these important advantages make harmonic Wigner sampling an attractive approach since an arbitrary number of initial conditions can be sampled after just a single evaluation of the molecular Hessian.[6,7]

The assumptions behind harmonic Wigner sampling remain valid for rigid molecules, but can become qualitatively incorrect when large-amplitude motions are present. Representative examples include low-barrier internal rotations, which cannot be adequately described by uncoupled normal-mode coordinates defined at a single equilibrium geometry. In general, displacements along torsion or bending modes can lead to large coupling to bond stretching modes, either in the potential energy term (when the modes are expressed in terms of Cartesian coordinates) or in the kinetic energy term (when the modes are expressed in terms of internal coordinates).[11,12] To alleviate the effects of this problem, *ad hoc* corrections such as freezing low frequency normal modes during sampling are often needed.[13,14] However, it is difficult to predict the effect of completely neglecting low frequency motions at the start on the overall dynamics and there are no well-established guidelines to apply such corrections.

In the present work, we use vibrational self-consistent field (VSCF) theory[15] to build the vibrational wave function of the molecule from which we build the VSCF Wigner distribution to sample initial conditions for TSH simulations. VSCF is still a relatively crude approximation for the vibrational wave function of a molecule and post-VSCF methods such as vibrational configuration interaction (VCI) are required to obtain quantitative agreement with vibrational spectroscopy data.[16–18] However, compared to the simple harmonic approximation, 1D VSCF already fully takes into account the anharmonicity of the individual normal modes while higher levels begin to include the interaction between the modes in an averaged manner. The VSCF Wigner distribution retains the mode separability which was key to the applicability of the harmonic Wigner distribution. Additionally, it admits a simple analytic form both in the harmonic basis and in the distributed Gaussian basis (DGB). The VSCF Wigner distribution is not strictly positive, but as we will show below, the negative regions for the vibrational ground state are negligible even for a highly anharmonic system when the vibrational wave function is centered around a single minimum.

An alternative to sampling from the Wigner function is to run classical MD simulations

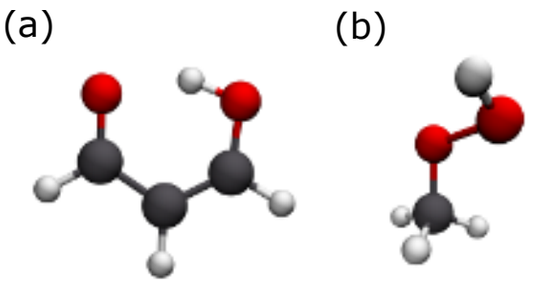

FIG. 1. Test systems: (a) malonadehyde and (b) methylhydroperoxide.

with a quantum thermostat (QT)[6,19,20] based on the generalized Langevin equation. A detailed review of such thermostats can be found in Ref. 20. The basic idea is to tune the thermostat parameters so that modes of different frequencies are maintained at distinct effective temperatures. These temperatures are selected so that, over a given frequency range, the resulting position and momentum variances are as close as possible to the values for the quantum harmonic oscillator.[19] Although tuning of the parameters is done for the harmonic oscillator, QT simulations perform well even for moderately anharmonic systems at higher temperatures. At very low temperatures, the thermostat fails to counteract the leakage of energy from high-frequency modes to low-frequency modes due to their large coupling.[19] Despite these limitations, QT has been successfully applied for sampling initial conditions for trajectory surface hopping dynamics,[6] with the main drawbacks being the need for long simulation times for equilibration and obtaining uncorrelated phase space points.[21]

In the following section, we give a brief introduction on two test systems with different levels of anharmonicity, malonaldehyde and methylhydroperoxide, shown in Fig. 1, which also serve to illustrate the problem with harmonic Wigner sampling. In Sec. III, we give an overview of VSCF and Wigner distributions and present analytical expressions for the VSCF Wigner distribution in the harmonic and distributed Gaussian basis. In Sec. V, we perform a detailed analysis of the differences between the sampling methods and their consequences in nonadiabatic dynamics simulations. These two examples demonstrate the applicability of the method and allow an assessment of its practical utility.

II. SYSTEMS

A. Malonaldehyde

Malonaldehyde is a six-membered ring system characterized by an intramolecular hydrogen bond of moderate strength. The barrier for H-transfer of ≈ 4 kcal/mol[22] implies that the wave function amplitude at the top of the barrier is negligibly small, allowing the initial wave function to be considered fully localized in a single minimum. Nevertheless, even near the minimum, the H-transfer potential is not harmonic, so including anharmonicity can influence the phase-space distribution, particularly that of the O−H bond length. It has been shown that anharmonicity affects the hydrogen-bond dynamics and leaves a clear signature in the OH-stretching region of the IR spectrum.[22,23] The extent to which the O−H bond length distribution influences the excited-state dynamics, however, has not yet been investigated.[24]

B. Methylhydroperoxide

Methylhydroperoxide (MHP) is a molecule where the failure of the harmonic approximation has been shown to result in very large errors when initial conditions are sampled from the harmonic Wigner distribution.[25] Here the observable of interest is the quantum yield of O−H *vs* O−O bond photodissociation. Prlj *et al.* have shown that, in the excitation window between 4.85 eV and 5.15 eV, harmonic Wigner sampling resulted in a quantum yield for O-H dissociation of 63.1% while the yield with QT sampling was 30.1%.[25] The source of this error is in the shape of the PES along two normal modes, the C−O−O−H torsional mode and the O−H stretching mode which are, respectively, the lowest (Q_1) and highest (Q_{15}) frequency modes of the molecule. This is illustrated in Fig. 2, where panels (a) and (b) show the 2D cut of the PES along the internal coordinates while panels (d) and (e) show cuts along the normal modes. One can see that away from the minimum, the directions of the torsion internal coordinate (yellow line) and normal mode (red line) are very different.

At the minimum, the Q_1 mode points along the tangent of the C−O−O−H torsion. However, as it is extended, the mode quickly deviates from pure torsion and couples to the O−H stretching coordinate, causing a sharp rise in potential energy. Because of this, the harmonic approximation drastically underestimates the energy of the molecule along a

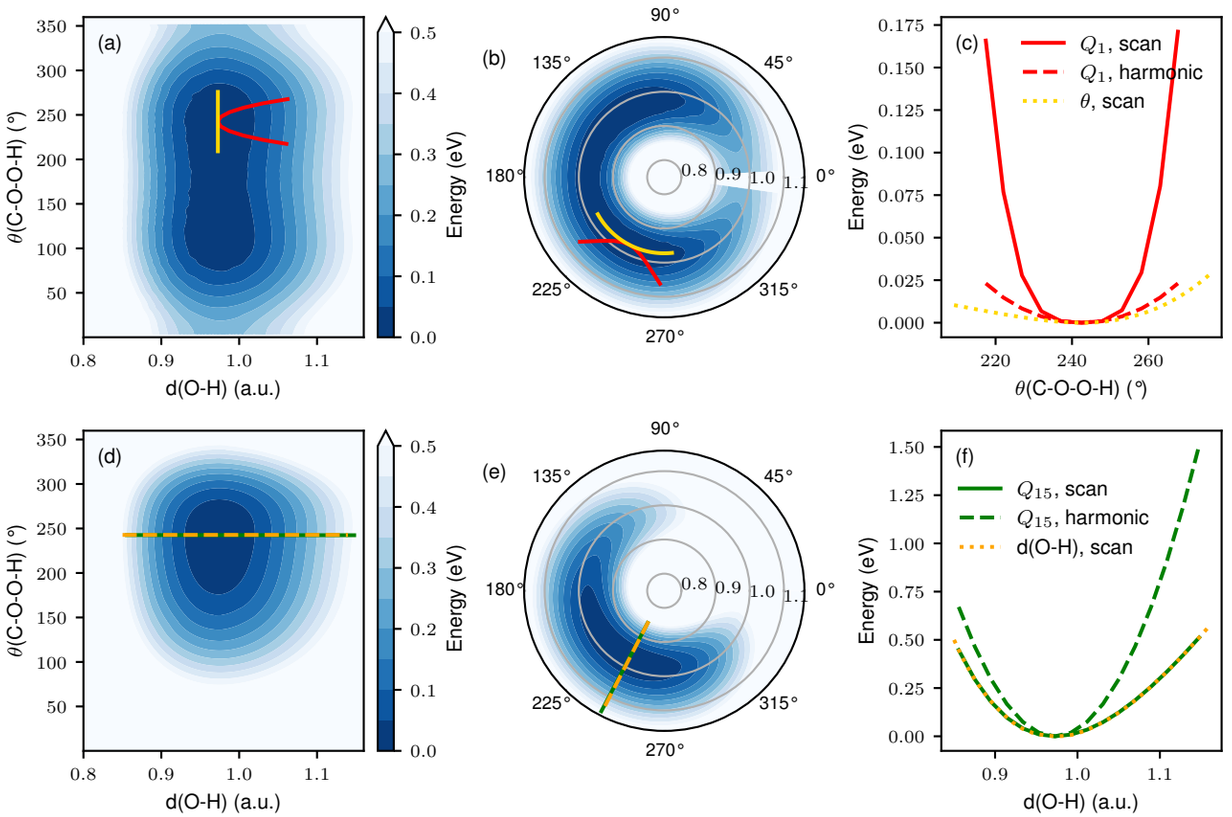

FIG. 2. 2D cuts of the MHP potential energy surface along the torsional and O−H stretch internal coordinates shown in Cartesian (a) and polar (b) representation and along the corresponding normal modes Q_1 and Q_{15} (d) and (e). (c) 1D cuts along the torsional internal coordinate (yellow line) and normal mode (red line). (f) 1D cuts along the bond stretch internal coordinate (orange line) and normal mode (green line).

scan of the Q_1 mode which, when sampling, results in geometries for which the O−H bond is artificially lengthened. Elongation of this bond lowers the transition energy of the $n'\sigma^*$ state. This state has a large oscillator strength and, thus, initial conditions with a heavily elongated O−H bond are more likely to be selected for initial excitation and have the biggest weights when determining photochemical observables.

III. THEORY

A. VSCF

We begin with a brief overview of the VSCF method, which provides the foundation for deriving the VSCF Wigner distribution. In VSCF theory, the vibrational wave function for the state $(n_1, ..., n_N)$ is written as a product of one-dimensional wave functions

$$\Psi_v(Q_1, ..., Q_N) = \prod_{i=1}^{N} \psi_i^{(n_i)}(Q_i)\,, \tag{1}$$

while the vibrational coupling is treated in a mean-field manner.[15] Thus, for a vibrational Hamiltonian $\hat{H}_v$, the effective Hamiltonian along the coordinate Q_i is given by

$$\hat{h}_i = \left\langle \prod_{j\neq i}^{N} \psi_j^{(n_j)} \middle| \hat{H}_v(Q_1, ..., Q_N) \middle| \prod_{j\neq i}^{N} \psi_j^{(n_j)} \right\rangle\,, \tag{2}$$

where the integration is done over the coordinates $Q_{j\neq i}$. The final vibrational wave function is obtained by iteratively solving a set of one-dimensional Schrödinger equations[15]

$$\left\langle \prod_{j\neq i}^{N} \psi_j^{(n_j)} \middle| \hat{H}_v(Q_1, ..., Q_N) \middle| \prod_{j\neq i}^{N} \psi_j^{(n_j)} \right\rangle \psi_i^{(n_i)}(Q_i) = \epsilon_i \psi_i^{(n_i)}(Q_i)\,. \tag{3}$$

In the following, we use mass and frequency scaled rectilinear normal coordinates and neglect the Watson coupling terms, so the vibrational Hamiltonian takes the form[26,27]

$$\hat{H}_v = -\frac{1}{2}\sum_{i=1}^{N} \omega_i \frac{\partial^2}{\partial Q_i^2} + V\left(Q_1, ..., Q_N\right)\,, \tag{4}$$

where ω_i is the harmonic frequency of mode i and $V\left(Q_1, ..., Q_N\right)$ is the potential energy operator. Atomic units ($\hbar = 1$) are used throughout the text. Constructing a PES by evaluating energies on an N-dimensional grid is computationally feasible only for small molecules. However, a hierarchical representation of the PES can be used[28,29]

$$V\left(Q_1, ..., Q_N\right) = \sum_{i=1}^{N} V_i^{(1)}(Q_i) + \sum_{i=1}^{N-1}\sum_{j>i}^{N} V_{ij}^{(2)}(Q_i, Q_j) + \dots\,, \tag{5}$$

where the intrinsic one-mode potentials are defined as

$$V_i^{(1)}(Q_i) = V\left(0, ..., Q_i, 0, ..., 0\right) \tag{6}$$

and intrinsic two-mode potentials are defined as

$$V_{ij}^{(2)}(Q_i) = V\left(0, ..., Q_i, ..., Q_j, ..., 0\right) - V_i^{(1)}(Q_i) - V_j^{(1)}(Q_j) \tag{7}$$

to avoid overcounting the one-mode contributions.[29,30] Higher-order intrinsic potentials are defined analogously. Truncating the hierarchical expansion at a low order leads to a substantial reduction of the number of points needed to obtain the potential energy on a grid. The order of mode couplings needed to obtain accurate results depends on the system as well as the coordinates used to describe vibrations.[31,32] However for most applications one doesn't need to go beyond three-mode representation,[18] and even two-mode representation usually only causes small errors, although higher order terms might be crucial to get accurate vibrational spectra.[32] A simple implementation requires $\sum_{n'=0}^{n} \binom{N}{n'} \times (N_g - 1)^{n'}$ potential energy evaluations for an n-mode representation, where N_g is the number of grid points along each dimension. However, approximations are available to reduce this number by using sparser grids and by evaluating higher order potentials only for relevant mode combinations.[27,33]

Once the PES is available, Eq. (3) can be solved. Two common basis sets for solving the VSCF equations are the harmonic oscillator basis and the distributed Gaussian basis. Their advantage is that, when a polynomial representation of PES is used (obtained by fitting to a grid), all the integrals needed to compute the Hamiltonian matrix elements in Eq. (4) can be obtained analytically.[33,34] In the harmonic oscillator basis set, the wave function takes the form

$$\psi(Q) = \sum_{\mu=0}^{\Theta} C_\mu \left[\frac{1}{\sqrt{2^\mu \mu!}} \left(\frac{1}{\pi}\right)^{1/4} \exp\left(-\frac{Q^2}{2}\right) H_\mu(Q) \right], \tag{8}$$

where H_μ is Hermite polynomial. In the distributed Gaussian basis, the wave function is written as

$$\psi(Q) = \sum_{\mu=0}^{\Theta} C_\mu \left(\frac{2A_\mu}{\pi}\right)^{1/4} \exp\left(-A_\mu (Q - Q_\mu)^2\right), \tag{9}$$

where Q_μ are the Gaussian centers and A_μ are the exponential parameters controlling their width. With the proper choice of these parameters, one can accurately describe the wave function while avoiding numerical problems arising from near linear dependence of the basis functions.[33,35] In the next subsection, we derive analytical expressions for the Wigner distribution from these two representations of the wave function.

B. Wigner distribution

The Wigner quasiprobability distribution function, for an N-dimensional system represented by a density matrix $\hat{\rho}$, is defined as[3]

$$W(\mathbf{Q},\mathbf{P}) = \left(\frac{1}{\pi}\right)^N \int_{-\infty}^{\infty} \langle \mathbf{Q}-\mathbf{y}|\hat{\rho}|\mathbf{Q}+\mathbf{y}\rangle \exp\left(2i\mathbf{P}\cdot\mathbf{y}\right) d\mathbf{y}\,. \tag{10}$$

To account for anharmonicity, we generated the Wigner distribution using the VSCF wave function (Eq. (1)). As in the VSCF wave function, the full VSCF Wigner distribution is given as the product of the one-mode Wigner distributions

$$W(\mathbf{Q},\mathbf{P}) = \left(\frac{1}{\pi}\right)^N \prod_{i=1}^{N} \int_{-\infty}^{\infty} \bar{\psi}_i^{(n_i)}\left(Q_i+y\right) \psi_i^{(n_i)}\left(Q_i-y\right) \exp\left(2iP_iy\right) dy\,. \tag{11}$$

In the harmonic oscillator basis (Eq. (8)), the one-mode Wigner function, $W(Q_i,P_i)$ can be written as

$$\begin{aligned} W(Q,P) = \frac{1}{\pi} \sum_{\mu=0}^{\Theta} \sum_{\nu=0}^{\Theta} C_\mu C_\nu \left(2^{\mu+\nu}\mu!\nu!\right)^{-1/2} \left(\frac{1}{\pi}\right)^{1/2} \times \\ \int_{-\infty}^{\infty} \Bigg[\exp\left(-\frac{1}{2}(Q+y)^2 - \frac{1}{2}(Q-y)^2 + 2iPy\right) \\ H_\mu\left(Q+y\right) H_\nu\left(Q-y\right) \Bigg] dy\,, \end{aligned} \tag{12}$$

where for simplicity we have dropped the mode index i. The integral in Eq. (12) was previously evaluated in Ref. 36, giving the expression:

$$\begin{aligned} W(Q,P) = \frac{1}{\pi} \sum_{\mu=0}^{\Theta} \sum_{\nu=0}^{\Theta} C_\mu C_\nu \left(\mu!\nu!2^{\mu+\nu}\right)^{1/2} \exp\left(-\left(Q^2+P^2\right)\right) \times \\ \sum_{\kappa=0}^{\min(\mu,\nu)} \frac{(-2)^{-\kappa}}{(\mu-\kappa)!(\nu-\kappa)!\kappa!} \left(Q-iP\right)^{\nu-\kappa} \left(Q+iP\right)^{\mu-\kappa}\,. \end{aligned} \tag{13}$$

If the wave function is expressed in the distributed Gaussian basis such as in Eq. (9), the one-mode Wigner function takes the form

$$\begin{aligned} W(Q,P) = \frac{1}{\pi} \sum_{\mu=0}^{\Theta} \sum_{\nu=0}^{\Theta} C_\mu C_\nu \left(\frac{2A_\mu}{\pi}\right)^{1/4} \left(\frac{2A_\nu}{\pi}\right)^{1/4} \times \\ \int_{-\infty}^{\infty} \exp\left[-A_\mu\left(Q+y-Q_\mu\right)^2\right] \exp\left[-A_\nu\left(Q-y-Q_\mu\right)^2\right] \exp\left(2iPy\right) dy\,, \end{aligned} \tag{14}$$

which can be expanded as

$$W(Q,P) = \frac{1}{\pi}\left(\frac{4}{\pi^2}\right)^{1/4} \sum_{\mu=0}^{\Theta}\sum_{\nu=0}^{\Theta} C_\mu C_\nu \left(A_\mu A_\nu\right)^{1/4} \times \exp\left(-Q^2(A_\mu + A_\nu) + 2Q(A_\mu Q_\mu + A_\nu Q_\nu) - \left(A_\mu Q_\mu^2 + A_\nu Q_\nu^2\right)\right) \times \int_{-\infty}^{\infty} \exp\left[-y^2(A_\mu + A_\nu) + y\left(2Q(A_\nu - A_\mu) + 2(A_\mu Q_\mu - A_\nu Q_\nu) + 2iP\right)\right] dy\,. \quad (15)$$

Identifying $\beta = A_\mu + A_\nu$ and $\gamma = (2Q(A_\nu - A_\mu) + 2(A_\mu Q_\mu - A_\nu Q_\nu) + 2iP)$, the integral in Eq. (15) can be written as

$$\begin{aligned}\int_{-\infty}^{\infty} \exp\left(-\beta y^2 + \gamma y\right) dy &= \exp\left(\frac{\gamma^2}{4\beta}\right) \int_{-\infty}^{\infty} \exp\left(-\beta\left(y - \frac{\gamma}{2\beta}\right)^2\right) dy \\ &= \sqrt{\frac{\pi}{\beta}} \exp\left(\frac{\gamma^2}{4\beta}\right)\,. \end{aligned} \quad (16)$$

Substituting into Eq. (15) gives the final expression for the one-mode Wigner distribution in the distributed Gaussian basis,

$$W(Q,P) = \frac{2^{1/2}}{\pi} \sum_{\mu=0}^{\Theta}\sum_{\nu=0}^{\Theta} C_\mu C_\nu \left(A_\mu A_\nu\right)^{1/4} \left(A_\mu + A_\nu\right)^{-1/2} \times \exp\left(-Q^2(A_\mu + A_\nu) + 2Q(A_\mu Q_\mu + A_\nu Q_\nu) - \left(A_\mu Q_\mu^2 + A_\nu Q_\nu^2\right)\right) \times \exp\left(\frac{\left(2Q(A_\nu - A_\mu) + 2(A_\mu Q_\mu - A_\nu Q_\nu) + 2iP\right)^2}{4(A_\mu + A_\nu)}\right)\,. \quad (17)$$

As with the harmonic basis, this analytical expression can be evaluated at virtually no computational cost. In conjunction with the fact that the Wigner distribution is written as a product of one-mode distributions which can be sampled independently, this means that the full cost of the sampling method is concentrated in the VSCF calculation.

From Eqs. (13) and (17), we see that the Wigner distributions generated from VSCF wave functions are no longer strictly positive even for the vibrational ground state. The question that arises is how to deal with the distribution's negative regions while sampling. One possibility is to simply ignore the negative regions by setting the probability of sampling from these regions to zero,[7,37]

$$W_+(Q,P) = \frac{\max\left(W(Q,P),0\right)}{\iint_{-\infty}^{\infty} \max\left(W(Q,P),0\right) dQdP}\,. \quad (18)$$

It should be noted that this approach is not generally applicable,[38] best illustrated by considering the example of a symmetric double well. In this case, the maximum of the ground

state Wigner function is at the origin even if the barrier is high enough for $|\Psi_v(Q)|^2$ to be vanishingly small near the origin. This in turn implies the existence of large negative regions around the origin so that their contributions cancel out when integrating over the momenta. In such a case, the probability distribution of the displacement would have a maximum at the origin (where the barrier is highest) when sampling from Eq. (18).

While this can pose serious problems for potentials with multiple minima, it has been shown that good results for low lying vibrational states can be obtained from VSCF calculations by restricting the PES to a single minimum.[39] A more general sampling strategy that works even in cases where the single-minimum approximation is not adequate, as well as for excited vibrational states is beyond the scope of this work.

IV. COMPUTATIONAL METHODS

A. VSCF calculations

We developed a code for constructing the PES and performing VSCF calculations in the harmonic oscillator and distributed Gaussian bases. These tools will be included in a future release of the ZagHop surface hopping code.[40] For both molecules, the distributed Gaussian basis was used. Grids of 17 points and 9×9 points were used for intrinsic 1D and 2D potentials, respectively. A total of 337 and 13777 (226 and 6961) were required for the constructions of 1D and 2D potentials for malonaldehyde (MHP). The grid range in frequency scaled normal coordinates was from -4 to 4. Since the C−O−O−H torsional mode of MHP in rectilinear normal coordinates significantly elongates the O−H bond, convergence issues occurred, and thus the normal coordinate was restricted to $[-2, 2]$. It should be noted that relatively simple algorithms for automatic determination of grid extensions such as the adaptive density-guided approach (ADGA)[33] are available, however for the systems involved in this work the default values were adequate except for a single, easily identified, mode. Prior to polynomial fitting, a cubic spline interpolation was used to create a fine grid of points. The 2D-VSCF wave functions obtained with such grids were compared to those obtained with denser, 33×33 point grids and the difference was negligible.

Ground state calculations for malonaldehyde and MHP were performed at the MP2/aug-cc-pVDZ level using the Turbomole 7.9. program package.[41–43]

B. Surface hopping simulations

Excited state calculations for malonaldehyde were performed at the SCS-ADC(2)/aug-cc-pVDZ level[44,45] using Turbomole 7.9.[41–43] with 8 excited singlet states included in the calculation. In total 10 000 phase space points were generated from the harmonic Wigner distribution and the 1D and 2D VSCF Wigner distributions using Eq. (11) and Eq. (17). Photoabsorption cross-sections were computed using the nuclear ensemble approach.[46,47] For the harmonic and 2D VSCF samples, trajectories were started from each state falling within an excitation window between 3.9 eV and 4.2 eV. A total of 3590 and 3995 trajectories were started for the harmonic and 2D VSCF samples, respectively. TSH simulations were performed using a development version of ZagHop.[40] The local diabatization version of the fewest switches surface hopping (LD-FSSH) algorithm was used,[48] with a nuclear propagation time step of 0.25 fs, and the energy-based decoherence correction from Ref. 49 was applied.

Following Prlj *et al.* calculations for MHP were performed at the XMS-CASPT2(8/6)/def2-SVDP level of theory using the BAGEL program package.[50,51] 20000 phase space points were sampled from the harmonic Wigner distribution, the harmonic Wigner distribution with the Q_1 mode frozen and from the 2D VSCF Wigner distribution. Initial conditions for trajectories were selected from an excitation window between 4.85 eV and 5.15 eV. A total of 2555, 2335 and 2923 trajectories were started for the harmonic, frozen Q_1 harmonic and 2D VSCF samples, respectively. The fewest-switches surface hopping simulations were performed using SHARC 2.1.[52,53] Further details can be found in Ref. 25.

To take into account the different transition probabilities of states falling within the chosen excitation window, each trajectory was given a weight proportional to its initial oscillator strength $w_i = \frac{f_i}{\sum_i f_i}$ and quantum yields were then evaluated as

$$\phi_{\text{prod}} = \sum_i w_i \phi_{\text{prod,i}} \tag{19}$$

where $\phi_{\text{prod,i}}$ is 1 if the trajectory ended with the chosen product and zero otherwise. All other quantities averaged over trajectories were computed analogously. Alternately, one can perform f-biased sampling, in which sampled points and transitions are selected (by rejection sampling) based on their oscillator strength. This produces a smaller number of trajectories, each with an equal weight. In the case of MHP, the state responsible for one of

the products (H product) rarely falls within the chosen energy window but has a very large oscillator strength. Because of this, the quantum yield is very sensitive to the sample size and the method chosen to evaluate the quantum yield, see the Supporting Information for a discussion on this topic.

V. RESULTS AND DISCUSSION

A. Malonaldehyde

For malonaldehyde, we first compare the bond length distributions generated from harmonic, 1D VSCF and 2D VSCF Wigner distributions. Distributions of the bond length for the different bonds in malonaldehyde are shown in Fig 3. The O−H bond is longer in both 1D and 2D VSCF samples compared to the harmonic Wigner sampling, while the distribution for the C=C bond is shifted to slightly higher values only for 2D VSCF. Both C−H bonds are elongated at the 1D VSCF level compared to the 2D VSCF sample which is closer to the harmonic Wigner sample. These results are not entirely unexpected since VSCF calculations with 1-mode representation of the PES often produce inaccurate anharmonic shifts and inclusion of mode-mode couplings is needed for accurate spectra.[32] Comparing to 3D VSCF calculations performed using the Molpro quantum chemistry program[54–57] (Table S1), we see that average bond lengths generated with 2D and 3D VSCF Wigner distributions at the MP2/cc-pVDZ level are in excellent agreement. Thus, at least for this molecule, it is safe to assume that there is no need to go beyond the 2-mode representation of the potential energy surface.

Photoabsorption cross-sections calculated for each of the samples are shown in Fig. 4. The first excited state at the ground state minimum geometry is a dark state of $n\pi^\star$ character and the first peak visible in the spectrum, centered at 4.7 eV, is assigned to the $\pi\pi^\star$ state which is the second excited state. The cross-section obtained using the 2D VSCF Wigner sample is slightly shifted compared to the harmonic and 1D VSCF Wigner samples. This can be explained by the fact that the C=C bond length distribution of the 2D VSCF sample is shifted in comparison to the distributions of 1D VSCF and harmonic samples (Fig. 3(b)). This bond extension is known to stabilize the $\pi\pi^\star$ with respect to the ground and first excited states, eventually leading to the S_2/S_1 conical intersection at a bond extension of

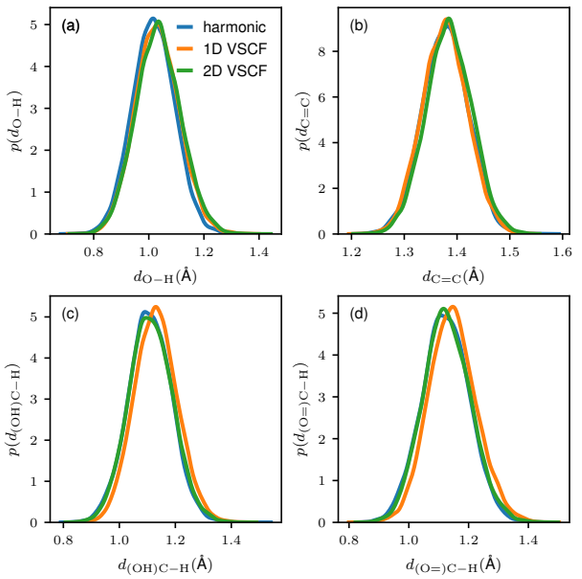

FIG. 3. Distribution of bond lengths in malonaldehyde: (a) O−H bond, (b) C=C bond, (c) C−H bond adjacent to the O–H group, and (d) C−H bond adjacent to the carbonyl group.

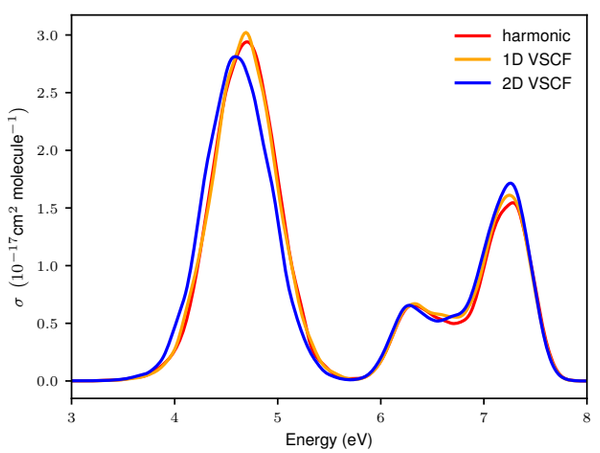

FIG. 4. Photoabsorption cross-section of malonaldehyde obtained with the nuclear ensemble approach using harmonic, 1D VSCF and 2D VSCF Wigner distributions.

only 0.07 Å.[24]

Although the difference in cross-sections is small at first glance, a shift of the spectrum could have a large influence on the sampling of initial conditions from a window at the low energy edge of a peak (as is often the target). In this case, inside an energy window between 3.9 eV to 4.2 eV the total number of states whose excitation energy falls within the

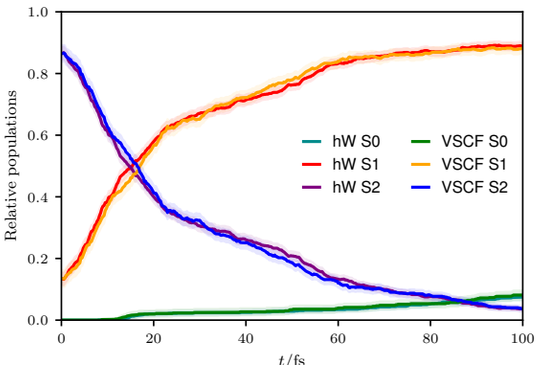

FIG. 5. Adiabatic state populations of malonaldehyde computed from initial conditions sampled using the harmonic Wigner (hW) and 2D VSCF Wigner distributions. Thick lines indicate oscillator-strength weighted populations obtained from all the points inside the energy window. The error bars represent 95% confidence intervals of populations obtained by running many f-biased simulations starting from the same initial phase space distribution.

window is similar for the 2D VSCF sample and the harmonic sample, as is the maximum oscillator strength. However, the summed intensity within the window is 1.58× larger for the 2D VSCF sample due to the $\pi\pi^\star$ state falling within this low energy window more often (Fig. S1). Consequently, the 2D VSCF sample produced on average 1.58× as many accepted trajectories when f-biased sampling was used.

TSH simulations were performed for all initial conditions in the selected energy window and the resulting adiabatic populations are shown in Fig. 5. Thick lines are the adiabatic populations computed by a posteriori weighting while the error bars (99% confidence intervals) are estimated by resampling 10000 f-biased runs from the whole sample and computing the adiabatic populations for each run. The adiabatic populations obtained with both samples are essentially identical. Thus, while the inclusion of anharmonic effects did affect the distribution of states within the chosen energy window, surface hopping dynamics is not sensitive to such changes. Also, contrary to what we will see for MHP, even a single f-biased sample yields reliable results that are close to those obtained with uniform sampling and a posteriori weighting of populations. This is due to a relatively high acceptance ratio, on average higher than 10% for both samples.

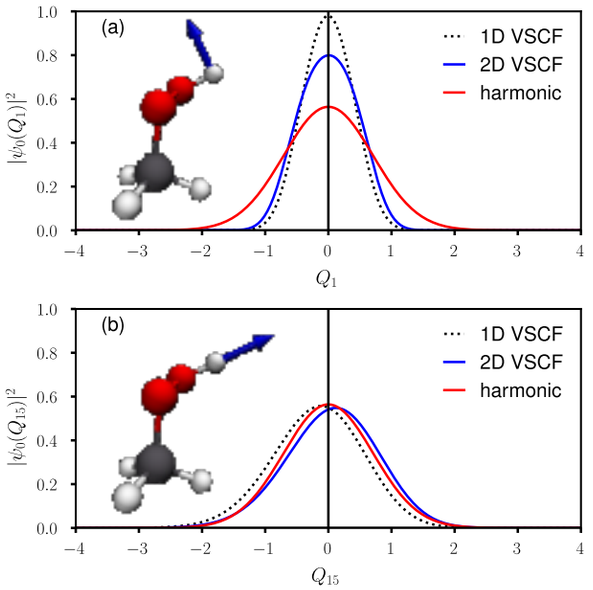

FIG. 6. Distributions of (a) the Q_1 (C−O−O−H torsion) and (b) the Q_{15} (O−H stretch) normal modes in MHP, computed using harmonic, 1D VSCF and 2D VSCF wave functions.

B. Methylhydroperoxide

To investigate the performance of VSCF Wigner sampling in this challenging example, we performed 2D VSCF calculations. For the Q_1 mode the 1D-VSCF potential is significantly steeper than the harmonic approximation resulting in a narrower wave function in the position representation. Extending to 2D VSCF, the effective potential along the Q_1 mode is more flat around the minimum than the 1D potential, but also rises steeply away from the minimum (Fig. S2). These differences in the potential are directly reflected in the $\psi(Q_1)$ wave functions used for generating the Wigner distribution, with the square modulus of the harmonic wave function being significantly broader than the other two, as shown in Fig. 6(a). In contrast, the wave functions for Q_{15} differ only subtly between the methods. At the 1D VSCF level, the wave function is shifted towards slightly longer bond lengths, as expected based on the difference between the harmonic and true 1D potential (Fig. 2(f)). However, this trend is reversed at the 2D VSCF level, Fig. 6(b). Upon inclusion of intrinsic two-mode potentials, the broadening of the distribution along the Q_1 mode (along which the O−H bond length increases) is partially compensated by a shift of the Q_{15} wave function towards lower O−H bond lengths.

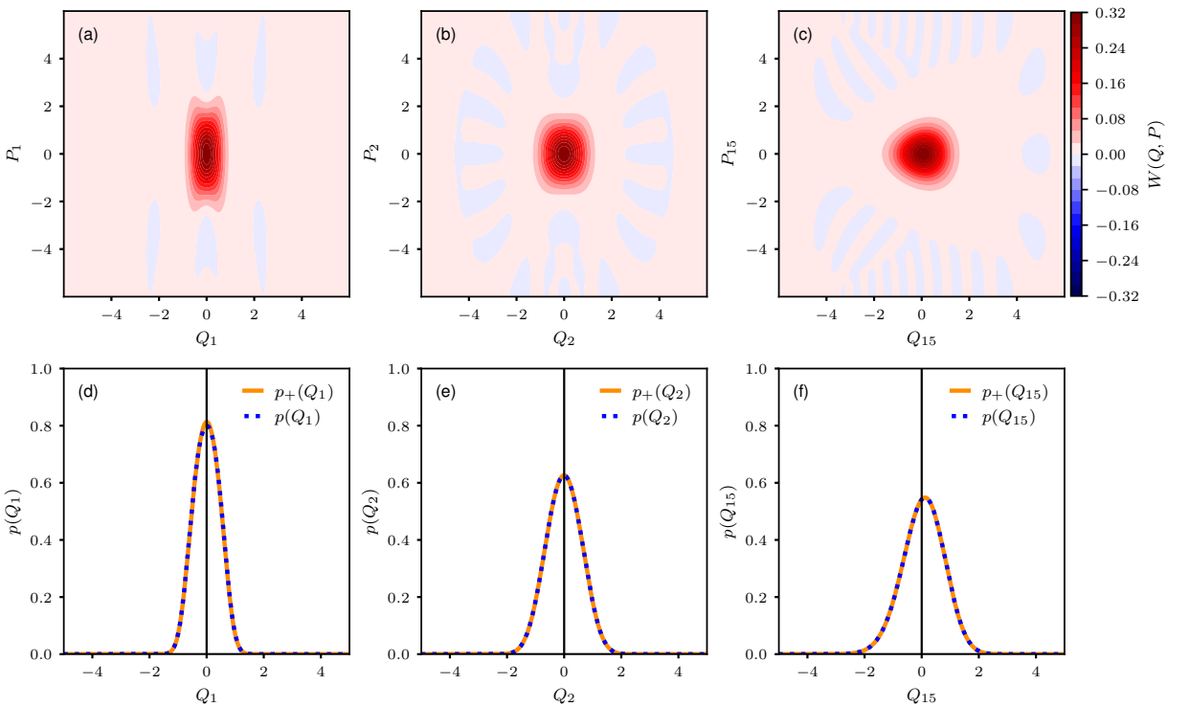

FIG. 7. Wigner distributions for (a) the C−O−O−H torsional mode, (b) the H−C−O−O torsional mode, and (c) the O−H stretching mode of MHP. Panels (d-f) show the corresponding normal mode displacement distributions obtained from the one-mode Wigner function ($p(Q)$) and from the positive-only W_+ distribution with negative regions set to zero ($p_+(Q)$).

At this point it is worth noting that all the Wigner distributions obtained from the ground state VSCF wave functions contain negative regions. To check whether it is valid to ignore those regions, as was done in Refs. 7 and 37 we compared the displacement (momentum) distributions obtained by numerically integrating the Wigner distribution over the momentum (displacement) with those obtained by integrating the W_+ distribution from Eq. (18). The Wigner functions and normal mode displacement distributions for select modes are shown in Fig. 7. The only (barely) noticeable difference is seen for the Q_1 mode, with W_+ producing a slightly narrower distribution for the normal coordinate, while the momentum distribution was slightly wider. Since ignoring the negative regions had little impact on the displacement and momentum distributions, we proceeded by sampling from the W_+ distribution. However, more work will be needed to establish a general strategy that is suitable for dealing with excited vibrational states and more anharmonic systems.

Next, we repeated the analyses of Ref. 25 for the harmonic Wigner distribution and the harmonic Wigner distribution with the torsional mode frozen (hereafter labeled harmonic*), and compared the results with those obtained from the VSCF Wigner distribution. The distribution of the C−O−O−H torsion angle and O−H bond length is shown in Fig. S3 and velocity distributions are shown in Fig. S4. The harmonic sample shows a high degree of correlation between the torsion angle and bond length, with bond length increasing as the torsion angle moves away from its equilibrium value. The harmonic* sample does not have the artificially elongated O−H bond, but the torsion angle distribution is exceedingly narrow since Q_1, the primary mode responsible for this torsion, is frozen. For the sample generated from the VSCF Wigner distribution, the C−O−O−H torsion angle distribution is somewhat narrower than that of the harmonic sample. However due to the shift of the O−H stretching mode wave function and the constraint of the torsional mode wave function in 2D VSCF calculations, the O−H bond length distribution is similar to that of the harmonic* sample, and thus to the bond length distribution of the sample generated by quantum thermostat in Ref. 25. The failure of the harmonic and harmonic* approximations is also visible in the photoabsorption cross-section shown in Fig. S5.

The main quantity of interest is the quantum yield. Fig. S6 shows a direct correlation between the initial O−H and O−O bond lengths and the final products of the trajectories both for the Wigner samples and the QT sample (on the other hand, there is little correlation between the initial velocities and the final product, Fig. S7). In Fig. 8, we compare the quantum yields of O−H and O−O bond dissociation (or the H and OH products respectively) for the three phase space sampling methods. After weighting the points according to Eq. (19) the quantum yields for H product formation are 58.7% for the full harmonic sample, 11.5% for the harmonic* sample and 26.6% for the 2D VSCF sample. In Fig. 8(d) bootstrap analysis shows that the difference in quantum yields is significant. As expected, the quantum yields for harmonic and harmonic* samples are comparable to those reported in Ref. 25. More importantly, the quantum yield for the 2D VSCF sample is closest to 30.1% obtained for quantum thermostat. This demonstrates that, despite the limitations of rectilinear normal coordinates and the single-minimum approximation, VSCF Wigner sampling effectively mitigates the main issue arising in the harmonic and harmonic* Wigner sampling.

Both the harmonic and VSCF Wigner distributions are obtained by making assumptions about the PES of the molecule. For any point $\mathbf{Q}_i$ sampled from these distributions, after

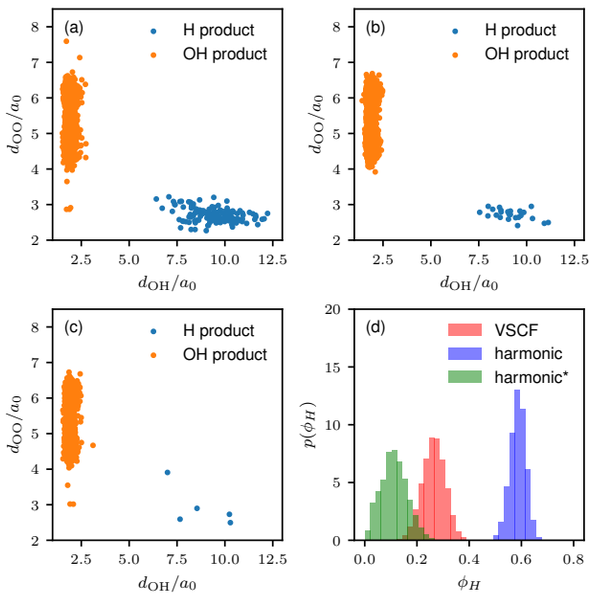

FIG. 8. Final O−O and O−H bond lengths for MHP trajectories started from (a) harmonic Wigner, (b) 2D VSCF Wigner and (c) frozen-torsion harmonic (harmonic*) Wigner samples. Trajectories with significantly lengthened O−H bonds were classified as H products. d) Distribution of H product quantum yields obtained by bootstrapping.

performing *ab initio* calculations, it is possible to quantify the error of the model PES as $\Delta E_{\text{err}}(\mathbf{Q}_i) = E_{model}(\mathbf{Q}_i) - E_{calc}(\mathbf{Q}_i)$. As expected, errors for the harmonic sample are significantly larger than for the 2D VSCF sample (Fig. 9(a)). Since $\Delta E_{\text{err}}(\mathbf{Q}_i)$ can be seen as a quantitative indicator of situations where a point was sampled from an area of configuration space where the model is not adequate, we can introduce a threshold t_{err} to remove points from a sample when $|\Delta E_{\text{err}}(\mathbf{Q}_i)| \geq t_{err}$. Fig. 9(b) examines the effect of lowering t_{err} on the H product quantum yield. For the harmonic sample, where the main source of the error in the model is the Q_1 mode, reducing t_{err} systematically removes points extended along this mode (and thus, with an elongated O−H bond), lowering the H product quantum yield. This reduction of the quantum yield does not converge to the values predicted from VSCF and QT samples, but instead continues declining to below 5%. On the other hand, t_{err} has a negligible effect on the 2D VSCF sample, indicating that the errors in the 2D VSCF sampling do not favor a particular product.

Fig. 9(b) can also be used to explain why simply freezing Q_1 during sampling does not result in the correct quantum yield. Both freezing modes and removing points with high

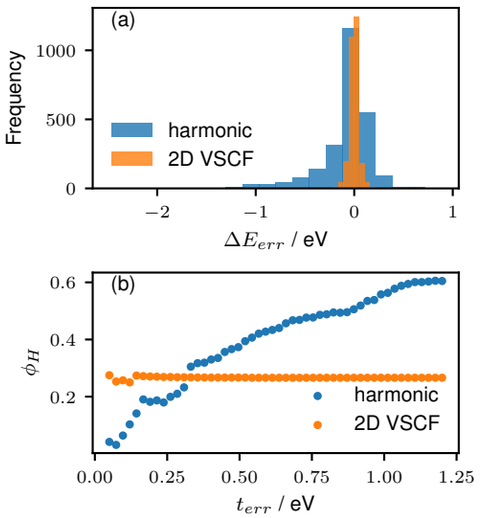

FIG. 9. (a) Errors, $\Delta E_{\mathrm{err}}(\mathbf{Q}_i)$, of the model PES relative to *ab initio* calculations for all phase space points sampled from the harmonic and 2D VSCF Wigner distributions of MPH. (b) Quantum yields estimated by including only trajectories whose initial geometries satisfy $\Delta E_{\mathrm{err}}(\mathbf{Q}_i) < t_{\mathrm{err}}$.

ΔE_{err} effectively removes parts of the phase space from consideration during sampling. While this does remove the most obviously bad geometries from the sample, the results cannot be systematically improved in this way, since the critical regions of phase space for specific pathways are not known *a priori*. In the case of MHP, at $t_{\mathrm{err}} \approx 0.4$ eV the quantum yield for the harmonic sample is close to the values obtained using QT or VSCF, but this is a result of error cancellation and not an indication that the harmonic sample is correct with this threshold value.

VI. CONCLUSION

In this work, we have presented a new method for sampling the phase space of molecules by employing the Wigner distribution based on VSCF calculations. The goal of the method is to efficiently and accurately sample initial conditions for TSH simulations of small to medium sized molecules while including the effect of zero point energy. The method keeps many of the advantages of the commonly employed harmonic Wigner sampling. At the same time, it overcomes the main drawback of the harmonic approximation, which breaks down when mode–mode couplings are important and the potential energy cannot be expressed as

a sum of harmonic normal mode terms.

The method was tested on two systems. For malonaldehyde, we see that using the 2D VSCF Wigner distribution slightly improves the distribution of bond lengths in the sample relative to harmonic sampling. However, this has only a small effect on the calculated photoabsorption cross-sections and on the subsequent TSH dynamics, suggesting that harmonic Wigner sampling may still be adequate for systems with moderate anharmonicity.

For MHP, where harmonic sampling generates many geometries with artificially extended bonds, 2D VSCF sampling proves to be very robust. The quantum yield of H product formation, 26.6%, agrees well with that obtained using the quantum thermostat approach (30.1%) and does not appear to result from error cancellation. This is notable given that the "problematic" mode involves rotation around a single bond, which is known to be challenging for VSCF.

In terms of cost, n-dimensional VSCF calculations scale roughly with the n^{th} power of the system size, meaning that the cost of a 1D VSCF calculation is comparable to the cost of a few numerical evaluations of the Hessian and 2D VSCF calculations are more expensive by a factor proportional to the number of normal modes of the system. For the small molecules and large samples used in the present work, fewer than one PES evaluation was needed per initial condition using 2D VSCF Wigner sampling, making the cost of sampling completely negligible in the overall computational cost of the nonadiabatic dynamics simulations.

Finally, an important advantage of the developed method is that its approximations are well-defined and a clear pathway for further improvements is available. Higher order representations of the PES can improve the accuracy of the VSCF calculation and vibrational configuration interaction (VCI) can be performed to remove the independent mode approximation. While Wigner sampling using VCI would drastically increase the cost of the calculation, it would be feasible for a molecule of a size similar to MHP and would provide a true benchmark against which both QT and VSCF sampling could be compared.

SUPPLEMENTARY MATERIAL

The supplementary material includes a comparison with 3D VSCF results and an analysis of oscillator strengths for malonaldehyde, additional method comparisons and analysis of generated velocities for MHP and a discussion on the accuracy of estimated quantum yields.

ACKNOWLEDGMENTS

We thank A. Prlj for assistance with the MHP calculations and for insightful discussions. We thank D. Hollas for the quantum thermostat initial conditions. R. C., J. O. and N. D. acknowledge funding from the Croatian Science Foundation (HRZZ grant no. HRZZ-IP-2022-10-4658). J. O. acknowledges the support from the PNRR MUR project PE0000023-NQSTI. This research was performed using the Advanced computing service provided by University of Zagreb University Computing Centre - SRCE.

DATA AVAILABILITY STATEMENT

The data that support the findings of this study are available from the corresponding author upon reasonable request.

REFERENCES

[1]J. C. Tully, J. Chem. Phys. **93**, 1061 (1990).

[2]M. Persico and G. Granucci, Theor. Chem. Acc. **133**, 1526 (2014).

[3]M. Hillery, R. F. O'Connell, M. O. Scully, and E. P. Wigner, Phys. Rep. **106**, 121 (1984).

[4]J. Beutier, D. Borgis, R. Vuilleumier, and S. Bonella, J. Chem. Phys. **141**, 084102 (2014).

[5]T. Plé, S. Huppert, F. Finocchi, P. Depondt, and S. Bonella, J. Chem. Phys. **151**, 114114 (2019).

[6]J. Suchan, D. Hollas, B. F. E. Curchod, and P. Slavíček, Faraday Discuss. **212**, 307 (2018).

[7]J. P. Zobel, J. J. Nogueira, and L. González, Phys. Chem. Chem. Phys. **21**, 13906 (2019).

[8]D. S. Tikhonov and Y. V. Vishnevskiy, Phys. Chem. Chem. Phys. **25**, 18406 (2023).

[9]N. Došlić and S. Bosanac, Mol. Phys. **90**, 599 (1997).

[10]S. Mukherjee and M. Barbatti, J. Chem. Theory Comput. **18**, 4109 (2022).

[11]E. L. Sibert, J. T. Hynes, and W. P. Reinhardt, J. Phys. Chem. **87**, 2032 (1983).

[12]A. B. McCoy, J. Phys. Chem. B **118**, 8286 (2014).

[13]O. Svoboda, M. Ončák, and P. Slavíček, J. Chem. Phys. **135**, 154301 (2011).

[14]L. Favero, G. Granucci, and M. Persico, Phys. Chem. Chem. Phys. **15**, 20651 (2013).

[15]J. M. Bowman, Acc. Chem. Res. **19**, 202 (1986).

[16]S. Carter, J. M. Bowman, and N. C. Handy, Theor. Chem. Acc **100**, 191 (1998).

[17]O. Christiansen, Phys. Chem. Chem. Phys. **9**, 2942 (2007).

[18]D. Oschetzki, M. Neff, P. Meier, F. Pfeiffer, and G. Rauhut, Croat. Chem. Acta **85**, 379 (2012).

[19]M. Ceriotti, G. Bussi, and M. Parrinello, Phys. Rev. Lett. **103**, 030603 (2009).

[20]M. Ceriotti, G. Bussi, and M. Parrinello, J. Chem. Theory Comput. **6**, 1170 (2010).

[21]H. Sheik, L. Grisanti, T. Ostojić, C. Lakmuang, B. Rossi, and A. Prlj, Phys. Chem. Chem. Phys. **27**, 18112 (2025).

[22]Y. Wang, B. J. Braams, J. M. Bowman, S. Carter, and D. P. Tew, J. Chem. Phys. **128**, 224314 (2008).

[23]N. Došlić and O. Kühn, Z. Phys. Chem. **217**, 1507 (2003).

[24]M. Sapunar, T. Ayari, and N. Došlić, Chem. Phys. **515**, 622 (2018).

[25]A. Prlj, D. Hollas, and B. F. E. Curchod, J. Phys. Chem. A **127**, 7400 (2023).

[26]J. O. Jung and R. B. Gerber, J. Chem. Phys. **105**, 10332 (1996).

[27]G. Rauhut, J. Chem. Phys. **121**, 9313 (2004).

[28]J. M. Bowman, S. Carter, and X. Huang, Int. Rev. Phys. Chem. **22**, 533 (2003).

[29]O. Christiansen, Phys. Chem. Chem. Phys. **14**, 6672 (2012).

[30]S. Carter, S. J. Culik, and J. M. Bowman, J. Chem. Phys. **107**, 10458 (1997).

[31]M. Schneider and G. Rauhut, J. Chem. Phys. **160**, 214118 (2024).

[32]E. L. Yang, J. J. Talbot, R. J. Spencer, and R. P. Steele, J. Chem. Phys. **159**, 204104 (2023).

[33]M. Sparta, D. Toffoli, and O. Christiansen, Theor. Chem. Acc. **123**, 413 (2009).

[34]A. Erba, J. Maul, M. Ferrabone, R. Dovesi, M. Rérat, and P. Carbonnière, J. Chem. Theory Comput. **15**, 3766 (2019).

[35]I. P. Hamilton and J. C. Light, J. Chem. Phys. **84**, 306 (1986).

[36]H. J. Groenewold, Physica **12**, 405 (1946).

[37]J. Yang, R. Dettori, J. P. F. Nunes, N. H. List, E. Biasin, M. Centurion, Z. Chen, A. A. Cordones, D. P. Deponte, T. F. Heinz, M. E. Kozina, K. Ledbetter, M.-F. Lin, A. M. Lindenberg, M. Mo, A. Nilsson, X. Shen, T. J. A. Wolf, D. Donadio, K. J. Gaffney, T. J. Martinez, and X. Wang, Nature **596**, 531 (2021).

[38]W. B. Case, Am. J. Phys. **76**, 937 (2008).

[39]S. Erfort, M. Tschöpe, G. Rauhut, X. Zeng, and D. P. Tew, J. Chem. Phys. **152**, 174306 (2020).

[40]"ZagHop, version 1.0, 2026, available from https://github.com/marin-sapunar/ZagHop,".

[41]"TURBOMOLE V7.9 2024, a development of University of Karlsruhe and Forschungszentrum Karlsruhe GmbH, 1989-2007, TURBOMOLE GmbH, since 2007; available from https://www.turbomole.org.".

[42]Y. J. Franzke, C. Holzer, J. H. Andersen, T. Begušić, F. Bruder, S. Coriani, F. Della Sala, E. Fabiano, D. A. Fedotov, S. Fürst, S. Gillhuber, R. Grotjahn, M. Kaupp, M. Kehry, M. Krstić, F. Mack, S. Majumdar, B. D. Nguyen, S. M. Parker, F. Pauly, A. Pausch, E. Perlt, G. S. Phun, A. Rajabi, D. Rappoport, B. Samal, T. Schrader, M. Sharma, E. Tapavicza, R. S. Treß, V. Voora, A. Wodyński, J. M. Yu, B. Zerulla, F. Furche, C. Hättig, M. Sierka, D. P. Tew, and F. Weigend, J. Chem. Theory Comput. **19**, 6859 (2023).

[43]C. Hättig and F. Weigend, J. Chem. Phys. **113**, 5154 (2000).

[44]J. Schirmer, Phys. Rev. A **26**, 2395 (1982).

[45]A. Hellweg, S. A. Grün, and C. Hättig, Phys. Chem. Chem. Phys. **10**, 4119 (2008).

[46]R. Crespo-Otero and M. Barbatti, Theor. Chem. Acc. **131**, 1237 (2012).

[47]D. Hollas and B. F. E. Curchod, J. Phys. Chem. A **128**, 8580 (2024).

[48]G. Granucci, M. Persico, and A. Toniolo, J. Chem. Phys. **114**, 10608 (2001).

[49]G. Granucci and M. Persico, J. Chem. Phys. **126**, 134114 (2007).

[50]T. Shiozaki, W. Gyorffy, P. Celani, and H.-J. Werner, J. Chem. Phys. **135**, 081106 (2011).

[51]T. Shiozaki, Wiley Interdiscip. Rev. Comput. Mol. Sci. **8**, e1331 (2018).

[52]M. Richter, P. Marquetand, J. González-Vázquez, I. Sola, and L. González, J. Chem. Theory Comput. **7**, 1253 (2011).

[53]S. Mai, P. Marquetand, and L. González, Wiley Interdiscip. Rev. Comput. Mol. Sci. **8**, e1370 (2018).

[54]H.-J. Werner, P. J. Knowles, P. Celani, W. Györffy, A. Hesselmann, D. Kats, G. Knizia, A. Köhn, T. Korona, D. Kreplin, R. Lindh, Q. Ma, F. R. Manby, A. Mitrushenkov, G. Rauhut, M. Schütz, K. R. Shamasundar, T. B. Adler, R. D. Amos, S. J. Bennie, A. Bernhardsson, A. Berning, J. A. Black, P. J. Bygrave, R. Cimiraglia, D. L. Cooper, D. Coughtrie, M. J. O. Deegan, A. J. Dobbyn, K. Doll, M. Dornbach, F. Eckert, S. Erfort, E. Goll, C. Hampel, G. Hetzer, J. G. Hill, M. Hodges, T. Hrenar, G. Jansen, C. Köppl, C. Kollmar, S. J. R. Lee, Y. Liu, A. W. Lloyd, R. A. Mata, A. J. May, B. Mussard, S. J. McNicholas, W. Meyer, T. F. Miller III, M. E. Mura, A. Nicklass, D. P. O'Neill, P. Palmieri, D. Peng, K. A. Peterson, K. Pflüger, R. Pitzer, I. Polyak, M. Reiher, J. O. Richardson,

J. B. Robinson, B. Schröder, M. Schwilk, T. Shiozaki, M. Sibaev, H. Stoll, A. J. Stone, R. Tarroni, T. Thorsteinsson, J. Toulouse, M. Wang, M. Welborn, and B. Ziegler, "Molpro, version 2024.3, a package of ab initio programs," See https://www.molpro.net.

[55]H.-J. Werner, P. J. Knowles, F. R. Manby, J. A. Black, K. Doll, A. Heßelmann, D. Kats, A. Köhn, T. Korona, D. A. Kreplin, Q. Ma, T. F. Miller, A. Mitrushchenkov, K. A. Peterson, I. Polyak, G. Rauhut, and M. Sibaev, J. Chem. Phys. **152**, 144107 (2020).

[56]T. Hrenar, G. Rauhut, and H.-J. Werner, J. Phys. Chem. A **110**, 2060 (2006).

[57]B. Ziegler and G. Rauhut, J. Chem. Phys. **144**, 114114 (2016).